Supplementary material for "Integer quantum Hall effect and enhanced g-factor in quantum confined Cd_3As_2 films" by R. Xiao *et al*

(Dated: July 21, 2022)

I. TEM OF ULTRATHIN Cd_3As_2 FILMS

Figure S1 shows the cross-sectional transmission electron microscopy (TEM) images of the three Cd_3As_2 devices studied with different thicknesses. TEM shows a good interface between GaSb and Cd_3As_2 , and a good crystalline quality of Cd_3As_2 . They can also confirm that the thicknesses of the measured Cd_3As_2 devices are 15 nm, 12 nm, and 10 nm. High resolution scanning transmission electron microscopy (STEM) was performed at 300 kV on a dual spherical aberration-corrected FEI Titan G2 60-300 S/TEM. All the STEM images were collected by using a high angle annular dark field (HAADF) detector with a collection angle of 50-100 mrad. Energy-dispersive X-ray spectroscopic (EDS) elemental maps of the sample surface were collected by using a SuperX EDS system under STEM mode which has four detectors surrounding the sample.

Cross-sectional TEM samples were prepared using a FEI Helios 660 focused ion beam (FIB) system. A thick protective amorphous carbon layer was deposited over the region of interest then Ga+ ions (30 kV then stepped down to 1 kV to avoid ion beam damage to the sample surface) were used in the FIB to make the samples electron transparent for TEM images.

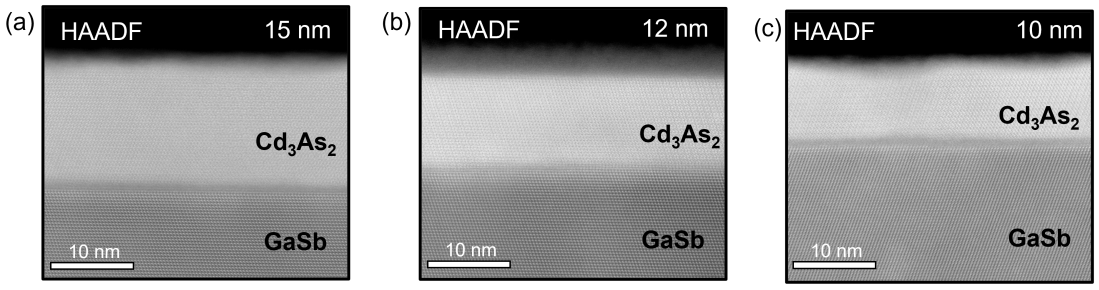

FIG. S1. Low-magnification cross-sectional HAADF-STEM image of ultrathin Cd_3As_2 films. (a), (b), (c) show Cd_3As_2 films with thicknesses of 15 nm, 12 nm and 10 nm, respectively.

II. THE IQHE IN Cd_3As_2 FILMS WITH DIFFERENT THICKNESSES: LONGITUDINAL AND HALL RESISTANCE DATA

Figure S2 shows the integer quantum Hall effect (IQHE) in Cd_3As_2 films with three different thicknesses 15 nm, 12 nm and 10 nm. Well-developed quantum Hall plateaus and near-zero ρ_{xx} can be observed for all three thicknesses,at $B = 9$ T and $T = 50$ mK

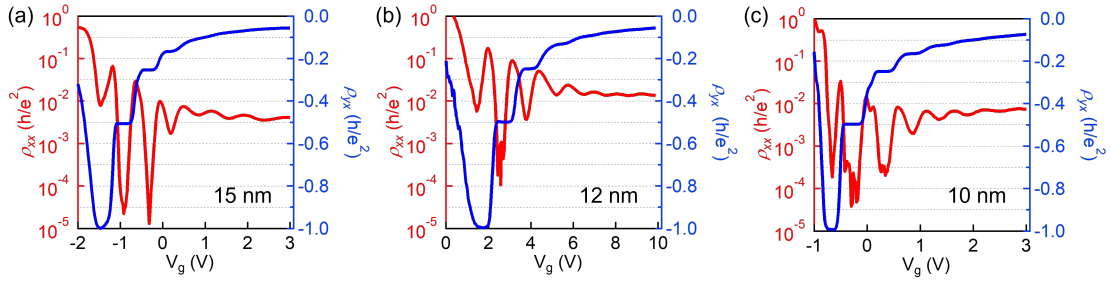

FIG. S2. The IQHE in Cd_3As_2 films with different thickness. (a), (b), (c) show gate voltage dependence of ρ_{xx} (red, left axis) and ρ_{xy} (blue, right axis) at $B = 9$ T and $T = 50$ mK of ultrathin Cd_3As_2 films with thicknesses of 15 nm, 12 nm and 10 nm respectively.

III. DETERMINING FILLING FACTORS USING THE DERIVATIVE OF ρ_{xx}

By combining $d\rho_{xx}/dV$ and ρ_{xy}(Fig.S3), we identify the values of gate voltage that correspond to the extrema in quantum oscillations, thus allowing us to reliably determine the value of the relevant filling factor. As shown in Table S1, only even filling factors including $\nu = 4, 6, 8, 10, 12$ are observed using this method.

IV. DETERMINATION OF FILLING FACTORS USING THE LANDAU LEVEL FAN DIAGRAM

Figure S4 shows the Landau level fan diagram with two different possible series of filling factors: (a) $\nu = 4, 6, 8, 10, 12$ and (b) $4, 6, 9, 11, 13$. The series of even filling factors (a) produces a more self-consistent Landau fan diagram with the different energy levels extrapolating to "zero." .

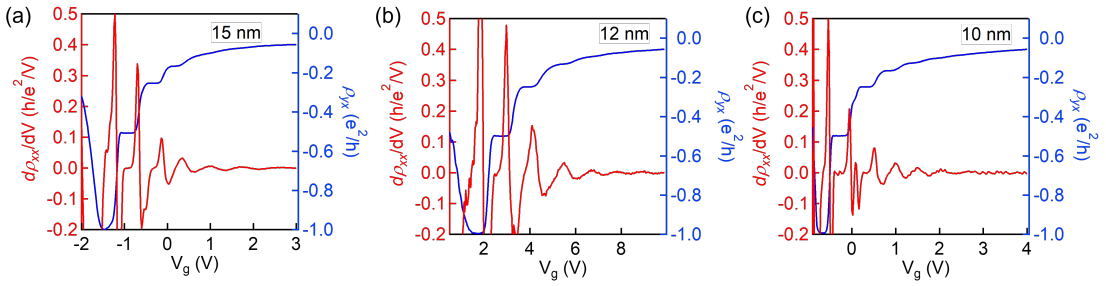

FIG. S3. The first derivative of ρ_{xx} of Cd_3As_2 films. (a), (b), (c) show gate voltage dependence of $d\rho_{xx}/dV$ (red, left axis), and ρ_{xy} (blue, right axis) at $B = 9$ T and $T = 50$ mK of untrathin Cd_3As_2 films with thicknesses of 15nm, 12 nm and 10 nm respectively.

V. TIGHT-BINDING MODEL OF Cd_3As_2

Based on the four-band $\mathbf{k}\cdot\mathbf{p}$ model of Cd_3As_2 near Γ point [1, 2], a tight-binding model with finite-range hopping is constructed by first substituting $\sin(k_i l_i)/l_i$ and $2(1-\cos(k_i l_i))/l_i^2$ for k_i and k_i^2, respectively, followed by an inverse Fourier transform. Here, $l_x = l_y = a = 12.633$Å and $l_z = c = 25.427$Å [3] are the lattice constants of a conventional 160-atom unit cell of Cd_3As_2. After the substitution, the $\mathbf{k}\cdot\mathbf{p}$ model becomes

$$\begin{aligned}\mathcal{H}(\mathbf{k}) =& C(\mathbf{k})\Gamma_0 + M(\mathbf{k})\Gamma_5 + \frac{\alpha_{E_u}}{a}\left[\sin(k_x a)\Gamma_3 - \sin(k_y a)\Gamma_4\right] \\ &+ \frac{2\lambda_{B_{2u}}}{a^2 c}\left[-\cos(k_x a) + \cos(k_y a)\right]\sin(k_z c)\Gamma_1 \\ &+ \frac{2\lambda_{B_{1u}}}{a^2 c}\sin(k_x a)\sin(k_y a)\sin(k_z c)\Gamma_2,\end{aligned} \tag{1}$$

where $C(\mathbf{k}) = C_0 + 2C_1[2-\cos(k_x a)-\cos(k_y a)]/a^2 + 2C_2[1-\cos(k_z c)]/c^2$, $M(\mathbf{k}) = -M_0 + 2M_1[2-\cos(k_x a)-\cos(k_y a)]/a^2 + 2M_2[1-\cos(k_z c)]/c^2$. Here, the spin-orbit coupled states $\mathcal{S} = \{|S_{J=\frac{1}{2}}, J_z = \frac{1}{2}\rangle, |P_{\frac{3}{2}}, \frac{3}{2}\rangle, |S_{\frac{1}{2}}, -\frac{1}{2}\rangle, |P_{\frac{3}{2}}, -\frac{3}{2}\rangle\}$ form the basis of the above Hamiltonian, $\Gamma_0 = \sigma_0 \otimes \tau_0$, $\Gamma_{1,2,3} = \sigma_{x,y,z} \otimes \tau_x$, $\Gamma_4 = \sigma_0 \otimes \tau_y$, and $\Gamma_5 = \sigma_0 \otimes \tau_z$ with σ's and τ's being defined in the spin and orbital spaces respectively, $\sigma_0 = \tau_0 = \mathrm{Id}_2$ and $\sigma_i = \tau_i, i = x, y, z$ are Pauli matrices. By performing an inverse Fourier transformation of trigonometric functions of $\mathbf{k}$, we can obtain the following tight-binding hopping model in a 3D tetragonal lattice $\mathcal{L}$,

$$H = \sum_{\mathbf{n},\mathbf{m}\in\mathcal{L};\alpha,\beta\in\mathcal{S}} \mathcal{H}_{(\mathbf{n},\alpha);(\mathbf{m},\beta)} c^\dagger_{(\mathbf{n},\alpha)} c_{(\mathbf{m},\beta)}, \tag{2}$$

where $c_{(\mathbf{n},\alpha)}$ is the annihilation operator for a spin-orbit coupled state $\alpha \in \mathcal{S}$ at the lattice site $\mathbf{n} = (n_x, n_y, n_z)$ and the sum over $\mathbf{m}$ runs up to the third nearest neighboring sites of $\mathbf{n}$.

15 nm					
Gate voltage (V)	$\rho_{xx}(h/e^2)$	$\rho_{yx}(h/e^2)$	$\sigma_{xx}(e^2/h)$	$\sigma_{xy}(e^2/h)$	Filling factor υ
0.18	0.0017	-0.1664	0.0625	-6.0086	6
0.86	0.0072	-0.1269	0.4456	-7.8535	8
1.54	0.0049	-0.1021	0.4733	-9.7752	10
2.38	0.0052	-0.0853	0.7074	-11.6868	12
12 nm					
Gate voltage (V)	$\rho_{xx}(h/e^2)$	$\rho_{yx}(h/e^2)$	$\sigma_{xx}(e^2/h)$	$\sigma_{xy}(e^2/h)$	Filling factor υ
5.2	0.0262	-0.1586	1.0152	-6.1388	6
6.54	0.0217	-0.1177	1.5162	-8.2171	8
7.66	0.0153	-0.0935	1.7064	-10.4140	10
8.64	0.0137	-0.0769	2.2532	-12.6016	12
10 nm					
Gate voltage (V)	$\rho_{xx}(h/e^2)$	$\rho_{yx}(h/e^2)$	$\sigma_{xx}(e^2/h)$	$\sigma_{xy}(e^2/h)$	Filling factor υ
0.86	0.0020	-0.1651	0.0749	-6.0543	6
1.34	0.0042	-0.1268	0.2639	-7.8799	8
1.9	0.0054	-0.1025	0.5143	-9.7289	10
2.5	0.0066	-0.0847	0.9098	-11.7291	12

FIG. Table S1. The determination of filling factors using $d\rho_{xx}/dV$.

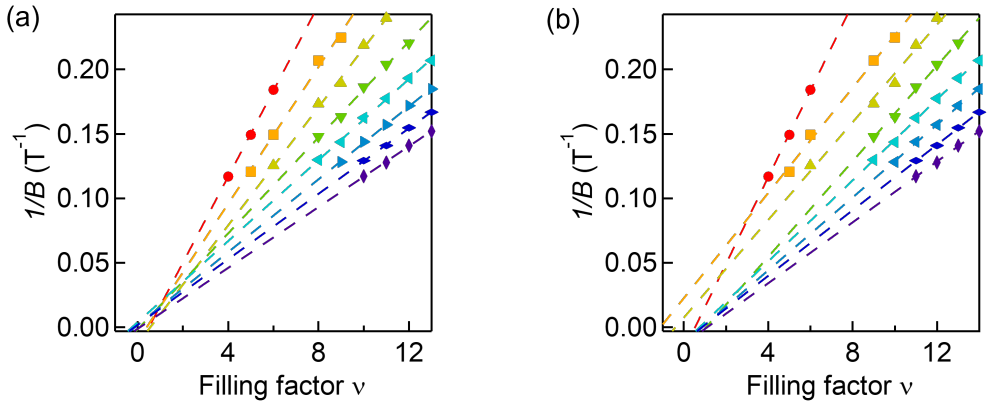

FIG. S4. The Landau level fan diagram of a 15 nm thick Cd_3As_2 thin film. The Landau fan diagrams are assigned using different series of filling factors (a) $\nu = 4, 6, 8, 10, 12$ and (b) $4, 6, 9, 11, 13$. The filling factor ν is used on the x axis, instead of the Landau index n, in order to distinguish different series of filling factors.

It is convenient to organize the kernel $\mathcal{H}_{(\mathbf{n},\alpha);(\mathbf{m},\beta)}$ in nested blocks. Each block is a 4-by-4 matrix describing the hopping from a given site $\mathbf{m}$ to a given site $\mathbf{n}$. Its matrix elements are labelled by the spin-orbit coupled basis α and β in $\mathcal{S}$.

Specifically, inverted bands and linear momentum spin-orbit couplings in the original $\mathbf{k}\cdot\mathbf{p}$ model give rise to on-site and nearest neighbor hoppings with the following non-vanishing blocks in the tight-binding model Hamiltonian,

$$
\begin{aligned}
\mathcal{H}_{\mathbf{n},\mathbf{n}} &= \begin{pmatrix} \mathcal{C}+\mathcal{M} & 0 & 0 & 0 \\ 0 & \mathcal{C}-\mathcal{M} & 0 & 0 \\ 0 & 0 & \mathcal{C}+\mathcal{M} & 0 \\ 0 & 0 & 0 & \mathcal{C}-\mathcal{M} \end{pmatrix}, \\
\mathcal{H}_{\mathbf{n},\mathbf{n}+\boldsymbol{\delta}_x} = \mathcal{H}^{\dagger}_{\mathbf{n}+\boldsymbol{\delta}_x,\mathbf{n}} &= \begin{pmatrix} -\frac{C_1+M_1}{a^2} & \frac{\alpha_{E_u}}{2\,\mathrm{i}\,a} & 0 & 0 \\ \frac{\alpha_{E_u}}{2\,\mathrm{i}\,a} & -\frac{C_1-M_1}{a^2} & 0 & 0 \\ 0 & 0 & -\frac{C_1+M_1}{a^2} & -\frac{\alpha_{E_u}}{2\,\mathrm{i}\,a} \\ 0 & 0 & -\frac{\alpha_{E_u}}{2\,\mathrm{i}\,a} & -\frac{C_1-M_1}{a^2} \end{pmatrix}, \\
\mathcal{H}_{\mathbf{n},\mathbf{n}+\boldsymbol{\delta}_y} = \mathcal{H}^{\dagger}_{\mathbf{n}+\boldsymbol{\delta}_y,\mathbf{n}} &= \begin{pmatrix} -\frac{C_1+M_1}{b^2} & \frac{\alpha_{E_u}}{2b} & 0 & 0 \\ -\frac{\alpha_{E_u}}{2b} & -\frac{C_1-M_1}{b^2} & 0 & 0 \\ 0 & 0 & -\frac{C_1+M_1}{b^2} & \frac{\alpha_{E_u}}{2b} \\ 0 & 0 & -\frac{\alpha_{E_u}}{2b} & -\frac{C_1-M_1}{b^2} \end{pmatrix}, \\
\mathcal{H}_{\mathbf{n},\mathbf{n}+\boldsymbol{\delta}_z} = \mathcal{H}^{\dagger}_{\mathbf{n}+\boldsymbol{\delta}_z,\mathbf{n}} &= \begin{pmatrix} -\frac{C_2+M_2}{c^2} & 0 & 0 & 0 \\ 0 & -\frac{C_2-M_2}{c^2} & 0 & 0 \\ 0 & 0 & -\frac{C_2+M_2}{c^2} & 0 \\ 0 & 0 & 0 & -\frac{C_2-M_2}{c^2} \end{pmatrix},
\end{aligned}
\tag{3}
$$

where $\mathcal{C} = C_0 + 2C_1(1/a^2 + 1/b^2) + 2C_2/c^2$ and $\mathcal{M} = -M_0 + 2M_1(1/a^2 + 1/b^2) + 2M_2/c^2$, $\boldsymbol{\delta}_x = (1,0,0)$, $\boldsymbol{\delta}_y = (0,1,0)$, and $\boldsymbol{\delta}_z = (0,0,1)$ are unit lattice basis vectors along x-, y-, and z directions of the lattice.

The cubic spin-orbit coupling terms in the original $\mathbf{k}\cdot\mathbf{p}$ model give rise to longer range

hoppings between up to the third nearest neighboring sites,

$$\mathcal{H}_{\mathbf{n},\mathbf{n}+\boldsymbol{\delta}_{xyz}^{+-+}} = \mathcal{H}_{\mathbf{n},\mathbf{n}+\boldsymbol{\delta}_{xyz}^{-++}} = \mathcal{H}_{\mathbf{n},\mathbf{n}+\boldsymbol{\delta}_{xyz}^{---}} = \mathcal{H}_{\mathbf{n},\mathbf{n}+\boldsymbol{\delta}_{xyz}^{++-}}$$

$$= \mathcal{H}^{\dagger}_{\mathbf{n}+\boldsymbol{\delta}_{xyz}^{+-+},\mathbf{n}} = \mathcal{H}^{\dagger}_{\mathbf{n}+\boldsymbol{\delta}_{xyz}^{-++},\mathbf{n}} = \mathcal{H}^{\dagger}_{\mathbf{n}+\boldsymbol{\delta}_{xyz}^{---},\mathbf{n}} = \mathcal{H}^{\dagger}_{\mathbf{n}+\boldsymbol{\delta}_{xyz}^{++-},\mathbf{n}} = \begin{pmatrix} 0 & 0 & 0 & -\frac{\lambda_{B_{1u}}}{8abc} \\ 0 & 0 & -\frac{\lambda_{B_{1u}}}{8abc} & 0 \\ 0 & \frac{\lambda_{B_{1u}}}{8abc} & 0 & 0 \\ \frac{\lambda_{B_{1u}}}{8abc} & 0 & 0 & 0 \end{pmatrix},$$

$$\mathcal{H}_{\mathbf{n},\mathbf{n}+\boldsymbol{\delta}_{xyz}^{00+}} = \mathcal{H}^{\dagger}_{\mathbf{n}+\boldsymbol{\delta}_{xyz}^{00+},\mathbf{n}} = \begin{pmatrix} 0 & 0 & 0 & \frac{\lambda_{B_{2u}}}{\mathrm{i}ca^2} - \frac{\lambda_{B_{2u}}}{\mathrm{i}cb^2} \\ 0 & 0 & \frac{\lambda_{B_{2u}}}{\mathrm{i}ca^2} - \frac{\lambda_{B_{2u}}}{\mathrm{i}cb^2} & 0 \\ 0 & \frac{\lambda_{B_{2u}}}{\mathrm{i}ca^2} - \frac{\lambda_{B_{2u}}}{\mathrm{i}cb^2} & 0 & 0 \\ \frac{\lambda_{B_{2u}}}{\mathrm{i}ca^2} - \frac{\lambda_{B_{2u}}}{\mathrm{i}cb^2} & 0 & 0 & 0 \end{pmatrix}, \tag{4}$$

$$\mathcal{H}_{\mathbf{n},\mathbf{n}+\boldsymbol{\delta}_{xyz}^{-0-}} = \mathcal{H}_{\mathbf{n},\mathbf{n}+\boldsymbol{\delta}_{xyz}^{+0-}} = \mathcal{H}^{\dagger}_{\mathbf{n}+\boldsymbol{\delta}_{xyz}^{-0-},\mathbf{n}} = \mathcal{H}^{\dagger}_{\mathbf{n}+\boldsymbol{\delta}_{xyz}^{+0-},\mathbf{n}} = \begin{pmatrix} 0 & 0 & 0 & \frac{\lambda_{B_{2u}}}{2\,\mathrm{i}ca^2} \\ 0 & 0 & \frac{\lambda_{B_{2u}}}{2\,\mathrm{i}ca^2} & 0 \\ 0 & \frac{\lambda_{B_{2u}}}{2\,\mathrm{i}ca^2} & 0 & 0 \\ \frac{\lambda_{B_{2u}}}{2\,\mathrm{i}ca^2} & 0 & 0 & 0 \end{pmatrix},$$

$$\mathcal{H}_{\mathbf{n},\mathbf{n}+\boldsymbol{\delta}_{xyz}^{0++}} = \mathcal{H}_{\mathbf{n},\mathbf{n}+\boldsymbol{\delta}_{xyz}^{0-+}} = \mathcal{H}^{\dagger}_{\mathbf{n}+\boldsymbol{\delta}_{xyz}^{0++},\mathbf{n}} = \mathcal{H}^{\dagger}_{\mathbf{n}+\boldsymbol{\delta}_{xyz}^{0-+},\mathbf{n}} = \begin{pmatrix} 0 & 0 & 0 & \frac{\lambda_{B_{2u}}}{2\,\mathrm{i}cb^2} \\ 0 & 0 & \frac{\lambda_{B_{2u}}}{2\,\mathrm{i}cb^2} & 0 \\ 0 & \frac{\lambda_{B_{2u}}}{2\,\mathrm{i}cb^2} & 0 & 0 \\ \frac{\lambda_{B_{2u}}}{2\,\mathrm{i}cb^2} & 0 & 0 & 0 \end{pmatrix},$$

where $\boldsymbol{\delta}_{xyz}^{pqr} = p\boldsymbol{\delta}_x + q\boldsymbol{\delta}_y + r\boldsymbol{\delta}_z$, $p, q, r \in \{-1, 0, +1\}$.

VI. QUANTUM HALL EFFECT AND LANDAU LEVELS

In this section, we derive a formula for Landau levels in thin films of Cd_3As_2. It has been used for analyzing the Landau fan diagrams mapped in the experiments.

Electrons in thin films of Cd_3As_2 form quasi-2D subbands with a subband gap because of the finite size confinement. Near the band gap, the pair of the lowest conduction subband and the highest valence subband is described by an anisotropic 2D massive Dirac Hamiltonian

$$H_{MD} = \Delta\sigma_z + v_\xi \Pi_\xi \sigma_x + v_\eta \Pi_\eta \sigma_y, \tag{5}$$

where Δ is the band gap due to finite-size confinement, v_ξ and v_η are velocities along two principal axes in the film plane. Each subband is two-fold degenerate. The kinetic

momentum $\Pi_i = p_i + eA_i$ is minimally coupled to the vector potential of the magnetic field.

In the presence of the magnetic field, the components of the kinetic momentum no long commute

$$[\Pi_\xi, \Pi_\eta] = -\,\mathrm{i}\,\hbar e[\partial_\xi A_\eta - \partial_\eta A_\xi] = -\,\mathrm{i}\,\hbar e B_\zeta, \tag{6}$$

where B_ζ is the component of the magnetic field perpendicular to the film.

It is useful to introduce the bosonic ladder operators $b, b^\dagger$ with

$$\begin{aligned} b =& \frac{\left(\frac{v_\xi}{v_\eta}\right)^{1/2}\Pi_\xi - \mathrm{i}\left(\frac{v_\eta}{v_\xi}\right)^{1/2}\Pi_\eta}{\sqrt{2\hbar e B_\zeta}}, \\ b^\dagger =& \frac{\left(\frac{v_\xi}{v_\eta}\right)^{1/2}\Pi_\xi + \mathrm{i}\left(\frac{v_\eta}{v_\xi}\right)^{1/2}\Pi_\eta}{\sqrt{2\hbar e B_\zeta}}, \end{aligned} \tag{7}$$

which satisfy $\left[b, b^\dagger\right] = 1$. Then the massive Dirac Hamiltonian in Eq. (5) can be rewritten as

$$H = \begin{pmatrix} \Delta & \sqrt{2\hbar e B_\zeta v_\xi v_\eta}\, b \\ \sqrt{2\hbar e B_\zeta v_\xi v_\eta}\, b^\dagger & -\Delta \end{pmatrix}. \tag{8}$$

Solve the Landau levels, we obtain

$$E_{LL}^n = \pm\sqrt{\Delta^2 + |n|(2\hbar e B_\zeta v_\xi v_\eta)}, n \in \mathbb{Z}. \tag{9}$$

Since the subbands are two-fold degenerate, the Landau levels with $n \neq 0$ are also doubly degenerate. The zeroth Landau levels are at $\pm|\Delta|$ depending on the sign of the gap. The bottom of the subbands reminiscent the surface Dirac cones on the top and bottom surfaces. If two degenerate subbands have opposite signs for the confinement gap Δ, two zeroth Landau levels will be singly degenerate at $\pm|\Delta|$ respectively.

If the subband gap is topologically trivial (e.g., by the hybridization of the surface states in thin films), there is a phase shift in the Landau level quantization. So the energy spectrum of the Landau levels associated to the conduction subbands are modified as

$$E_{LL}^n = \sqrt{\Delta^2 + (n+\gamma)(2\hbar e B_\zeta v_\xi v_\eta)}, n \geq 0, \tag{10}$$

and all the Landau level are doubly degenerated. When $\Delta^2 \gg (2\hbar e B_\zeta v_\xi v_\eta)$, by Taylor expansion, we have

$$E_{LL}^n \approx \Delta + \frac{(n+\gamma)(2\hbar e B_\zeta v_\xi v_\eta)}{2\Delta}, n \geq 0, \tag{11}$$

If we focus on the topologically trivial conduction subband, with a quadratic dispersion near the subband bottom, the Hamiltonian is

$$H = E_b + \frac{\Pi_\xi^2}{2m_\xi} + \frac{\Pi_\eta^2}{2m_\eta}, \tag{12}$$

where $m_\xi = \Delta/v_\xi^2$ and $m_\eta = \Delta/v_\eta^2$. The parameter m_ξ and m_η are effective band mass along the principal axes. E_b is the energy of the subband edge, which can be identified to Δ up to an additive constant. If the zero energy reference point is chosen in the middle of the mass gap, $E_b = \Delta$. The Landau level ladder operators are defined same as in Eq. 7 but represented in terms of effective mass as

$$\begin{aligned} b =& \frac{\left(\frac{m_\eta}{m_\xi}\right)^{1/4}\Pi_\xi - \mathrm{i}\left(\frac{m_\xi}{m_\eta}\right)^{1/4}\Pi_\eta}{\sqrt{2\hbar e B_\zeta}}, \\ b^\dagger =& \frac{\left(\frac{m_\eta}{m_\xi}\right)^{1/4}\Pi_\xi + \mathrm{i}\left(\frac{m_\xi}{m_\eta}\right)^{1/4}\Pi_\eta}{\sqrt{2\hbar e B_\zeta}}. \end{aligned} \tag{13}$$

The Landau levels are at

$$E_{LL}^n = E_b + \left(n + \frac{1}{2}\right)\hbar\omega^*, \tag{14}$$

where $\omega^* = \frac{eB_\zeta}{m^*}$, and $m^* = \sqrt{m_\xi m_\eta} = \frac{\Delta}{v_\xi v_\eta}$. The angular frequency ω^* is the cyclotron frequency, and the mass m^* is an effective mass for the cyclotron motion despite of the anisotropy of the subband dispersion. The effective cyclotron mass can also be extracted from quantum oscillation measurements, which will be reported else where. From the experiment measurements, one is able to identify two effective masses in thin films with n-doping, which has been attributed to the surface states and bulk subbands respectively. However, comparison to first principles calculations, the values only agree up to a factor of 2 to 3, which requires further studies in the future. Compare Eq. 11 and 14, we can identify $\gamma = \frac{1}{2}$ for purely quadratic dispersing bands.

There is an ambiguity in reducing the massive Dirac band dispersion (Eq. 5) to quadratic dispersion (Eq. 12) for the minimal coupling. In the absence of the magnetic field, Eq. 12) has the same spectrum as the Taylor expansion of the spectrum of Eq. 5 up to quadratic terms. In the presence of the magnetic field, they differ by another quadratic term arising

due to the non commutativity of the kinetic momentum Π_ξ and Π_η.

$$\begin{aligned}\Delta E =&\frac{1}{2\Delta}v_\xi v_\eta \,\mathrm{i}\,[\Pi_\xi,\Pi_\eta]\\ =&\frac{1}{2\Delta}v_\xi v_\eta \hbar e B_\zeta = \frac{1}{2}\hbar\omega^*.\end{aligned} \tag{15}$$

This is a quantum effect, which accounts for the relative shift of the spectrum of the Landau levels by $\frac{1}{2}\hbar\omega^*$ in Eq. 9 and Eq. 14. There is an alternative perspective to reconcile this ambiguity. For quadratic conduction band, one may attribute this additional energy shift to the quantum correction to the orbital magnetic moment from the valence band. The net effect of this quantum correction can be captured as an effective Zeeman coupling with an anomalous g-factor for the conduction band (in addition to the Zeeman shift of the spin magnetic moment where $g_0 = 2$). In fact, not only the bands relevant to the Dirac Hamiltonian, but also other near by bands (e.g., the light hole band and the split-off band) may contribute a non-negligible correction to the anomalous g-factor. To take in that in to account, we propose the following formula

$$E^n_{LL} =\sqrt{\Delta^2 + (n+\gamma)(2\hbar e B_\zeta v_\xi v_\eta)} + \frac{1}{2}g_{\mathrm{eff},\zeta}\mu_B B_\zeta, n \geq 0, \tag{16}$$

to fit the Landau levels measured in the experiments, where $g_{\mathrm{eff},\zeta} = g_0 + 2g'$ consists of the spin Zeeman effect and the orbital magnetic moment corrections.

VII. EFFECTIVE g-FACTOR OF Cd_3As_2

In this section we combine symmetry analysis, perturbative methods, and first-principle result to understand the thickness dependence of the effective g-factor of Cd_3As_2 film under a magnetic field along the [112]-direction. To take into account of the bulk band inversion and surface states arising from bulk Dirac crossing in Cd_3As_2, we generalize the derivation of the band g-factors in semiconductors [4, 5] by applying perturbation method to a generalized "Kane model" of Cd_3As_2 containing Dirac crossings. Then, we consider finite size effect and discuss the thickness dependence of the g-factor.

In Cd_3As_2, the bulk Dirac nodes arise from a pair of doubly degenerated inverted bands consistsing of Cd s-orbitals and As p-orbitals, which belongs to the irreducible representations (irreps) $|\Gamma^-_{6,(1)}\rangle = |S_{J=\frac{1}{2}}, J_z = \pm\frac{1}{2}\rangle$ and $|\Gamma^-_7\rangle = |P_{\frac{3}{2}}, \pm\frac{3}{2}\rangle$. There are another two doubly degenerated bands $|\Gamma^-_{6,(2)}\rangle = |P_{\frac{3}{2}}, \pm\frac{1}{2}\rangle$, $|\Gamma^+_6\rangle = |P_{\frac{1}{2}}, \pm\frac{1}{2}\rangle$, consisting of As p-orbitals.

$|\Gamma_7^-\rangle$and $|\Gamma_{6,(2)}^-\rangle$ are often referred to as the heavy hole and light hole bands, respectively, and $|\Gamma_6^+\rangle$ is referred to as the split-off bands. In these basis, analogous to the Kane model of semiconductors[5], an eight-band $\mathbf{k}\cdot\mathbf{p}$ model can be written as

$$H_{\mathbf{k}} = \left[E_{n,\mathbf{0}} + \frac{\hbar^2\mathbf{k}^2}{2m}\right] + \frac{\hbar}{m}\mathbf{k}\cdot\hat{\tilde{\mathbf{p}}} + \hat{\Delta}. \tag{17}$$

Here, $\hat{\tilde{\mathbf{p}}} = \mathbf{p} + (g_0\mu_B/c)\,\mathbf{s}\times(\nabla V_0)$, $\Delta = (g\mu_B/mc)[\mathbf{s}\times(\nabla V_0)]\cdot\mathbf{p}$, V_0 is the periodic potential, and $\mathbf{s}$ is the electron spin operator. The quantum number n is a spin-orbital index labelling the Bloch wave functions $\psi_{n,\mathbf{k}}(\mathbf{r}) = \exp[\mathrm{i}\,\mathbf{k}\cdot\mathbf{r}]u_{n,\mathbf{k}}(\mathbf{r})$. The matrix element of $\mathcal{H}_{\mathbf{k}}$ can be evaluated as $\mathcal{H}_{n,n'}(\mathbf{k}) = \langle u_n|H_{\mathbf{k}}|u_{n'}\rangle$, where

$$\{|u_n\rangle\} = \left\{|\Gamma_{6,(1)}^-\rangle, |\Gamma_7^-\rangle, |\Gamma_{6,(2)}^-\rangle, |\Gamma_6^+\rangle\right\}. \tag{18}$$

We shall denote $\{|u_\nu\rangle\} = \left\{|\Gamma_{6,(1)}^-\rangle, |\Gamma_{7,(1)}^-\rangle\right\}$ with Greek letters for the spin-orbital index of the bands that span the Hilbert space where the four band Dirac Hamiltonian is defined.

To reduce the Hamiltonian in Eq. (17) over $\{|u_n\rangle\}$ to an effective Hamiltonian over the subspace $\{|u_\nu\rangle\}$, we shall take the last two terms in Eq. (17) as perturbations. Up to second order perturbation, we obtain the effective Hamiltonian

$$\begin{aligned}\mathcal{H}^{\mathrm{eff}}_{\nu,\nu'}(\mathbf{k}) = &\left[E_{\nu,\mathbf{0}} + \frac{\hbar^2\mathbf{k}^2}{2m}\right] + \frac{\hbar}{m}\mathbf{k}\cdot\hat{\tilde{\mathbf{p}}}_{\nu,\nu'} + \hat{\Delta}_{\nu,\nu'} \\ &+ \frac{\hbar^2}{m^2}\sum_{n\neq\nu}\frac{1}{2}\left(\frac{1}{E_{\nu,\mathbf{0}} - E_{n,\mathbf{0}}} + \frac{1}{E_{\nu',\mathbf{0}} - E_{n,\mathbf{0}}}\right)\left(\mathbf{k}\cdot\hat{\tilde{\mathbf{p}}}_{\nu,n}\right)\left(\mathbf{k}\cdot\hat{\tilde{\mathbf{p}}}_{n,\nu'}\right) \\ &+ \sum_{n\neq\nu}\frac{1}{2}\left(\frac{1}{E_{\nu,\mathbf{0}} - E_{n,\mathbf{0}}} + \frac{1}{E_{\nu',\mathbf{0}} - E_{n,\mathbf{0}}}\right)\left[\hat{\Delta}_{\nu,n}\hat{\Delta}_{n,\nu'}\right].\end{aligned} \tag{19}$$

The first order terms come from the diagonal subblock $\mathcal{H}^{(1)}_{\nu,\nu'}(\mathbf{k}) = \langle u_\nu|\hbar\mathbf{k}\cdot\hat{\tilde{\mathbf{p}}}/m + \hat{\Delta}|u_{\nu'}\rangle$. The second order terms come from the off-diagonal blocks coupling the subspace $|u_\nu\rangle$ to the subspace $|u_{n\neq\nu}\rangle$. In usual semiconductors, it is the second order term in second line that renormalizes the the band mass, and gives rise to the anomalous g-factor, $2g'$, due to the orbital motions.

In the presence of the magnetic field, the magnetic field couples to both spin and orbital degrees of freedom. For the spin part, we have a Zeeman term

$$\mathcal{H}^{Z,s}_{\nu,\nu'} = g_0\mu_B(\mathbf{s}_{\nu,\nu'}/\hbar)\cdot\mathbf{B}\,. \tag{20}$$

For the orbital part, the magnetic field minimally coupled to the orbital motion according to the Peierls substitution $\hbar\mathbf{k}\to\boldsymbol{\pi} = -\,\mathrm{i}\,\hbar\nabla + e\,\mathbf{A}$. It gives rise to a term of orbital Zeeman

coupling from the second order term in Eq. (17) because of the non-commutativity among the operator components π_i as well as the matrices $\hat{\tilde{p}}^j$.

$$\begin{aligned}
\mathcal{H}^{Z,o}_{\nu,\nu'} =&\frac{1}{m^2}\sum_{n\neq\nu}\frac{1}{2}\left(\frac{1}{E_{\nu,\mathbf{0}}-E_{n,\mathbf{0}}}+\frac{1}{E_{\nu',\mathbf{0}}-E_{n,\mathbf{0}}}\right)\frac{1}{2}\left[\pi_i,\pi_j\right]\hat{\tilde{p}}^i_{\nu,n}\hat{\tilde{p}}^j_{n,\nu'}\\
=&\frac{-\,\mathrm{i}\,\hbar e}{2m^2}\sum_{n\neq\nu}\frac{1}{2}\left(\frac{1}{E_{\nu,\mathbf{0}}-E_{n,\mathbf{0}}}+\frac{1}{E_{\nu',\mathbf{0}}-E_{n,\mathbf{0}}}\right)\epsilon_{ijl}\hat{\tilde{p}}^i_{\nu,n}\hat{\tilde{p}}^j_{n,\nu'}B^l\\
=&\hat{g}'_{l;\nu,\nu'}\mu_B B^l,\\
\hat{g}'_{l;\nu,\nu'} =&\frac{-\,\mathrm{i}}{m}\sum_{n\neq\nu}\frac{1}{2}\left(\frac{1}{E_{\nu,\mathbf{0}}-E_{n,\mathbf{0}}}+\frac{1}{E_{\nu',\mathbf{0}}-E_{n,\mathbf{0}}}\right)\epsilon_{ijl}\hat{\tilde{p}}^i_{\nu,n}\hat{\tilde{p}}^j_{n,\nu'}.
\end{aligned}\tag{21}$$

Now we shall estimate the anomalous g-factor in [112]-oriented Cd_3As_2 thin films with a magnetic field perpendicular to the film, $\mathbf{B}=B_\zeta\hat{\zeta}$ with $\hat{\zeta}$ the unit vector along [112]. The quasi-2D bands in thin films arise from the split bulk subbands and the surface states as shown in Fig. 3(e) in the main text. Near the bottom of the lowest conduction band c_1, the states originate from hybridized surface states which do not belong to definitive irreps of bulk symmetry. The symmetry character of the rest nearby subbands at $\bar{\Gamma}$ is similar to that of the corresponding bulk bands from which they split. To apply Eq. (21) for quasi-2D bands in thin films, we shall take $\nu\in\{c_1,v_1\}$ and $n\in\{c_2,c_3,\ldots,v_2,v_3,\ldots\}$, where c_i and v_i denote respectively the i-th conduction and the i-th valence band counted from the charge neutral point.

To estimate the value of $\hat{g}'_\zeta$, one approximates $\hat{\tilde{\mathbf{p}}}\approx\mathbf{p}$ for off-diagonal matrix elements. The surface of the film break the translation symmetry along ζ-direction and the inversion symmetry, while the mirror reflection M_η remains a good symmetry ($\hat{\eta}=(1,-1,0)/\sqrt{2}$). M_η has the matrix representation $\pm\mathrm{i}\hat{\eta}\cdot\boldsymbol{\sigma}$ in $\Gamma^\pm_{6,7}$. As Cd_3As_2 is only weakly break the cubic symmetry, we assume all three mirror reflections (related to M_η by 3-fold rotations along ζ-axis) are also approximately good symmetries. Therefore, we have

$$\begin{aligned}
\hat{\tilde{p}}^\xi_{n,\nu} =&\frac{1}{2}D_{n,\nu}[(1+\omega)\sigma^x+(\omega+1)\sigma^y+2\omega^*\sigma^z],\\
\hat{\tilde{p}}^\eta_{n,\nu} =&\frac{1}{2\mathrm{i}}D_{n,\nu}(1-\omega)(\sigma^x-\sigma^y),\\
\hat{\tilde{p}}^\xi_{\nu,n}\hat{\tilde{p}}^\eta_{n,\nu}-\hat{\tilde{p}}^\eta_{\nu,n}\hat{\tilde{p}}^\xi_{n,\nu} =&\mathrm{i}\sqrt{3}|D_{n,\nu}|^2(\sigma^x+\sigma^y+\sigma^z).
\end{aligned}\tag{22}$$

where $\omega=\exp[2\pi\mathrm{i}/3]$ and $D_{n,\nu}$ is a c-number.

Substituting matrix elements for $\hat{\tilde{p}}^j_{n,\nu}$ in Eq. (21), we obtain the g-factor for the lowest

conduction band with a magnetic field along ζ-direction

$$g'_{\zeta;c_1} = \frac{3}{m} \sum_n \frac{|D_{n,c_1}|}{E_{c_1,\bar{\Gamma}} - E_{n,\bar{\Gamma}}}. \tag{23}$$

The sum is taken over $n \in \{c_2, c_3, \ldots, v_2, v_3, \ldots\}$. Notice that, the highest valence band v_1 is not included in the sum, because the spin-orbit coupling effect has been fully considered in the massive Dirac Hamiltonian in Eq. (5).

The thickness dependence of the g-factor arises from the thickness dependence of $E_{n,\bar{\Gamma}}$. As the subbands $n \neq c_1, v_1$ are derived from the bulk bands, their energy at $\bar{\Gamma}$ has a thickness dependence which can be obtained by expanding the bulk band dispersion relations with respect to k_ζ, i.e., $E_{n,\mathbf{0}} + M_n k_\zeta^2 + D_n k_\zeta^4 + \ldots$. In Fig. 3(e), we observe that for a 13 nm film, most subbands are almost quadratically dispersing but v_2. So We use parabolic band approximation for $n \neq v_2$, and keep up to quartic term for v_2 subband to capture its non-monotonic dispersion relation near $\bar{\Gamma}$. The band parameters E_n, M_n, D_n are fitted to the band structure of first principles calculations. Taking $|D_{n,c_1}|$ as fitting parameters, we obtain the thickness dependence of the g-factor in Cd_3As_2 thin films From the symmetry perspective, the dominant contribution to the anomalous g-factor may come from v_2. In Fig. 3 (f) of the main text, we consider $n = v_2$ in Eq. (23), and the matrix element $|D_{v_2,c_1}|$ is determined by the asymptotic value of the g-factor in the thick film limit.

[1] Z. Wang, H. Weng, Q. Wu, X. Dai, and Z. Fang, Three-dimensional dirac semimetal and quantum transport in cd_3as_2, Phys. Rev. B **88**, 125427 (2013).

[2] S. Baidya and D. Vanderbilt, First-principles theory of the Dirac semimetal Cd_3As_2 under Zeeman magnetic field, Phys. Rev. B **102**, 165115 (2020).

[3] M. N. Ali, Q. Gibson, S. Jeon, B. B. Zhou, A. Yazdani, and R. J. Cava, The crystal and electronic structures of Cd_3As_2, the three-dimensional electronic analogue of graphene, Inorganic Chemistry **53**, 4062 (2014).

[4] L. M. Roth, B. Lax, and S. Zwerdling, Theory of optical magneto-absorption effects in semiconductors, Phys. Rev. **114**, 90 (1959).

[5] R. Winkler, *Spin-Orbit Coupling Effects in Two-Dimensional Electron Systems* (Springer, 2003) pp. 18–20.